Traveling waves in developing cerebellar cortex mediated by asymmetrically connected Purkinje cells

Alanna J. Watt, Hermann Cuntz, Masahiro Mori, Zoltan Nusser, P. Jesper Sjöström & Michael Häusser

Supplementary Figures

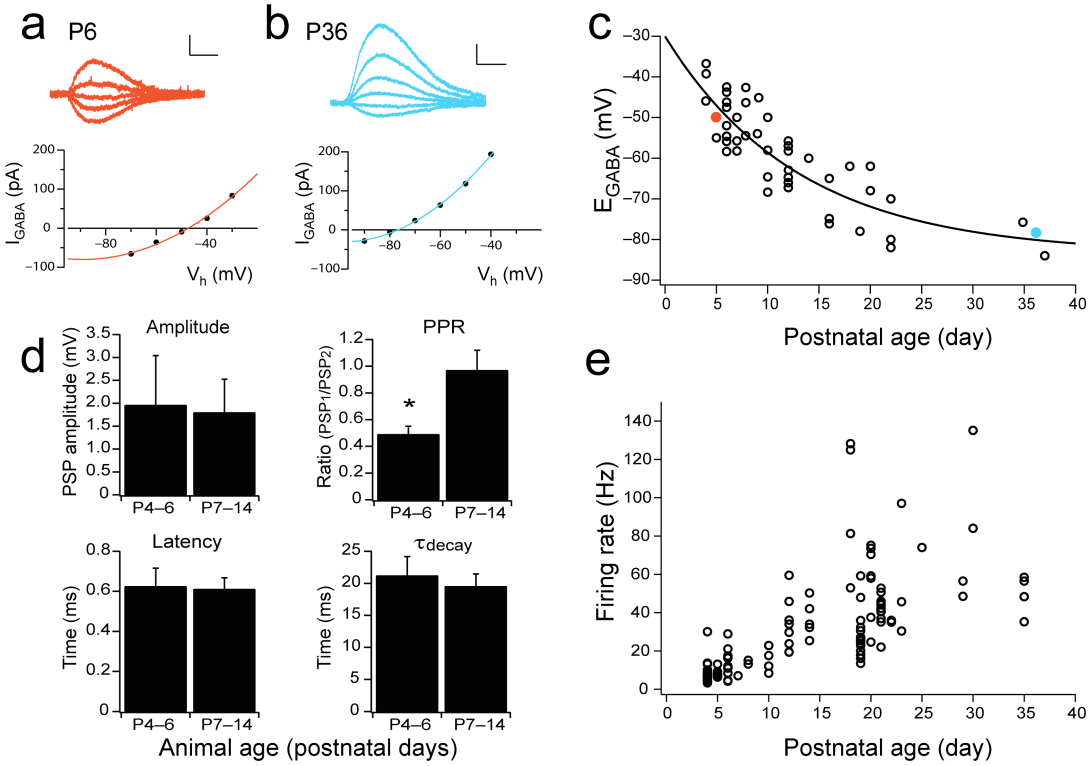

Supplementary Figure 1. Developmental changes in Purkinje Cells

(**a**) GABA-evoked currents recorded in a P6 Purkinje cell using gramicidin perforated-patch recordings (see Supplementary Methods). Example traces at different holding potentials are superimposed (top), with the respective peak GABA-evoked current amplitudes plotted below. Scale bar, 50 pA, 100 ms. (**b**) GABA-evoked currents recorded in a P36 Purkinje cell. Scale bar, 50 pA, 100 ms. (**c**) The GABA reversal potential (E_{GABA}) is depolarizing in the first week, but shifts to hyperpolarized values during the second postnatal week. Examples in panels (a) and (b) are indicated with red and blue closed circles, respectively. (**d**) Most synaptic properties exhibit no age-dependence when comparing data from 1-week-old (P4 – P6) and 2-week-old (P7 – P14) animals. There were no significant differences for PSP amplitude (n = 7/7, P4 – 6/P7 – P14; P = 0.90), latency (n = 9/12; P = 0.89), or τ_{decay} (n = 9/12; P = 0.63). However, there was significantly more paired-pulse depression in P4 – 6 animals (n = 18/6; P = 0.009). PSP amplitude was recorded with symmetrical Cl^- internal solution. Values are mean ± s.e.m. (**e**) Spontaneous firing rate is lower in young animals and increases during development. Firing rates were measured using cell-attached patch or extracellular recordings.

Nature Neuroscience: doi:10.1038/nn.2285

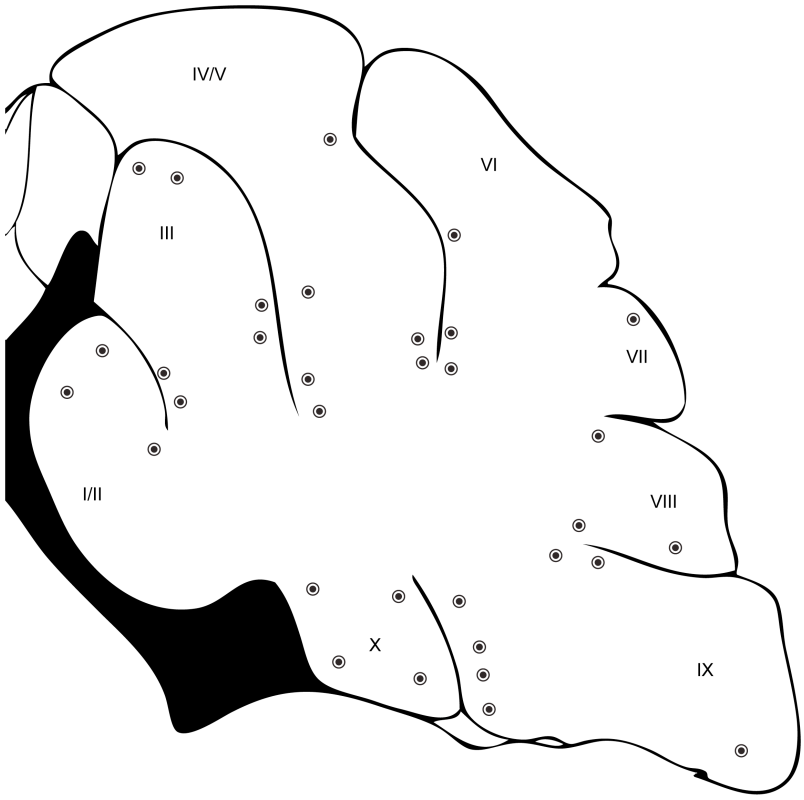

Supplementary Figure 2. Location of analyzed Purkinje cells within folia

Schematic sagittal section indicating the location of Purkinje cells whose axon collaterals were analyzed anatomically. Individual dots represent the location within the folia of 1 – 4 Purkinje cells. Adapted with permission from Ref. 1.

Nature Neuroscience: doi:10.1038/nn.2285

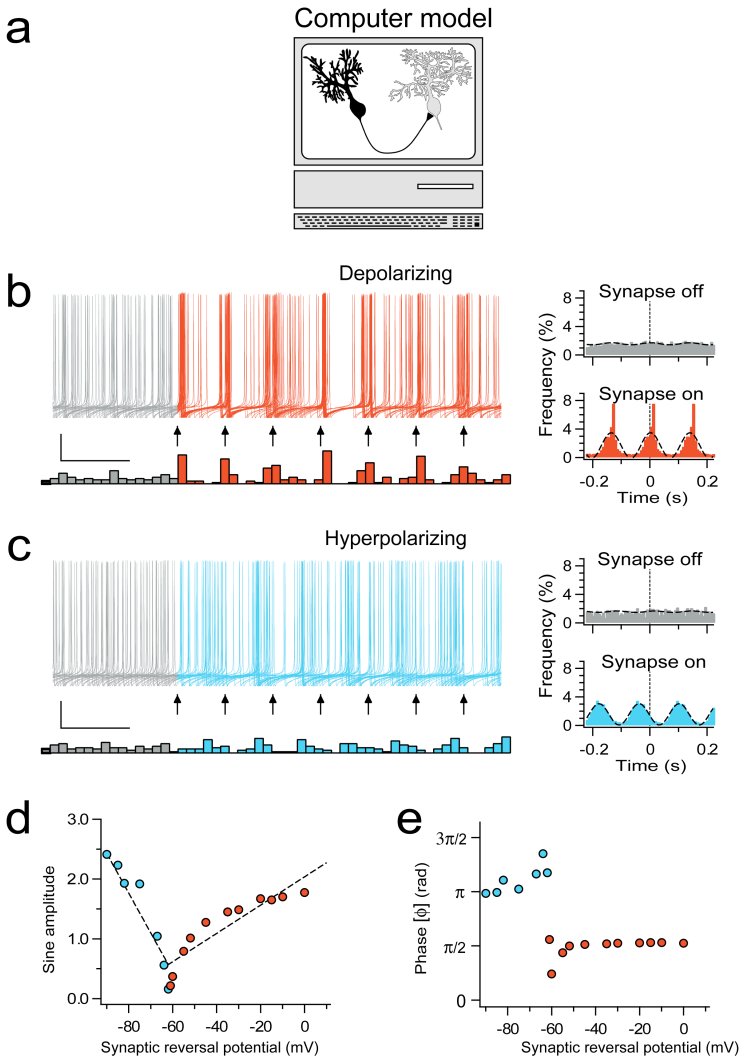

Supplementary Figure 3. Tuning the model

(**a**) Simulations of a connected pair of Purkinje cells were based on a published Purkinje cell model[2], and were carried out using NEURON[3] (see **Supplementary Methods**). (**b**) Similar to the dynamic clamp experiments (Fig. 4), turning on the synaptic connection (gray/red transition) resulted in the emergence of structured spiking patterns (top: 30 overlaid sweeps; bottom: spike histogram). After a baseline period, 7 Hz trains of 73 synaptic stimuli were delivered (first 7 indicated by arrows). Turning on this depolarizing synapse (g_{syn} = 0.8 nS; E_{rev} = 0 mV; firing rate: 6.9 Hz; see **Supplementary Methods**) caused correlated activity and postsynaptic entrainment (compare cross-correlograms inset top right and bottom right). Scale bar (top and bottom): 10 mV or 200 APs, 200 ms. (**c**) Switching on a hyperpolarizing synapse (E_{rev} = –80 mV) also resulted in structured spiking (top: 30 overlaid sweeps; bottom: spike histogram; rate: 6.9 Hz). However, as with the dynamic clamp experiments (Fig. 4), the phase of entrainment was different (compare inset bottom right to inset b). (**d**) The degree of entrainment (cf. b, c) was strongest for the most hyperpolarizing and depolarizing synaptic reversal potentials (blue: E_{rev} < –60 mV; red: otherwise), in good qualitative agreement with conductance clamp results (Fig. 4). (**e**) While hyperpolarizing and depolarizing synaptic reversal potentials both resulted in entrainment of the postsynaptic Purkinje cell (cf. b, c, d), the phase was different.

Nature Neuroscience: doi:10.1038/nn.2285

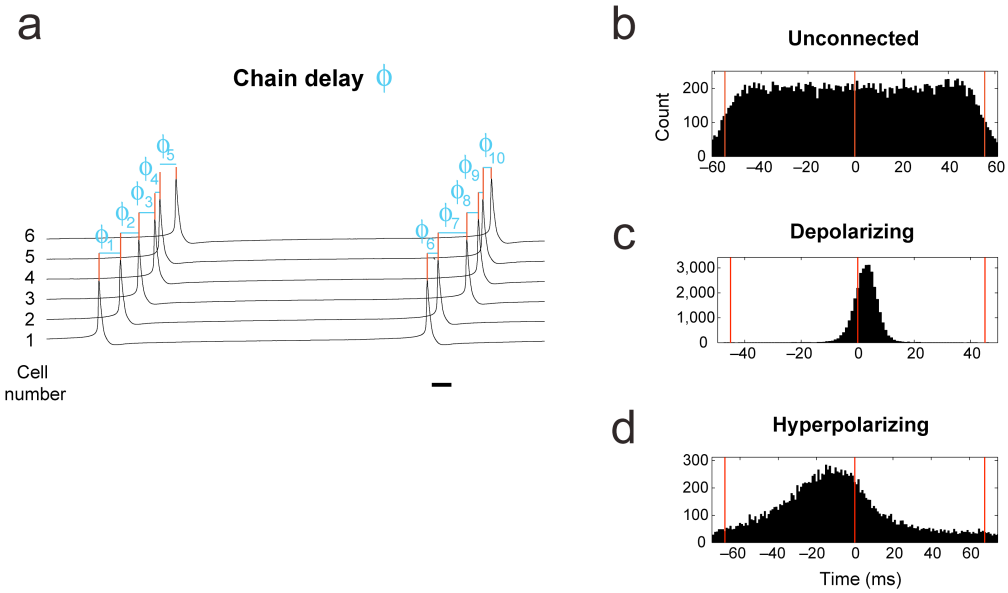

Supplementary Figure 4. Chain delay analysis of waves

(**a**) The chain delay (ϕ) measures the time between nearest spikes in neighboring cells, as illustrated (see Supplementary Methods and Supplementary Fig. 3). Scale bar, 5 ms. (**b**) Chain delay histogram for a model network of 50 unconnected Purkinje cells. Vertical red lines indicate the average interspike intervals. The broad, flat distribution indicates the absence of correlated firing across neighboring Purkinje cells. (**c**) When connected by depolarizing synapses, a sharp, positive peak was observed in the chain delay distribution, indicating the wave travels from the apex to the base of the lobule. (**d**) Hyperpolarizing synapses resulted in a chain delay peak that was broader than for depolarizing synapses (cf. c). The peak was negative, showing that waves move in the opposite direction.

Nature Neuroscience: doi:10.1038/nn.2285

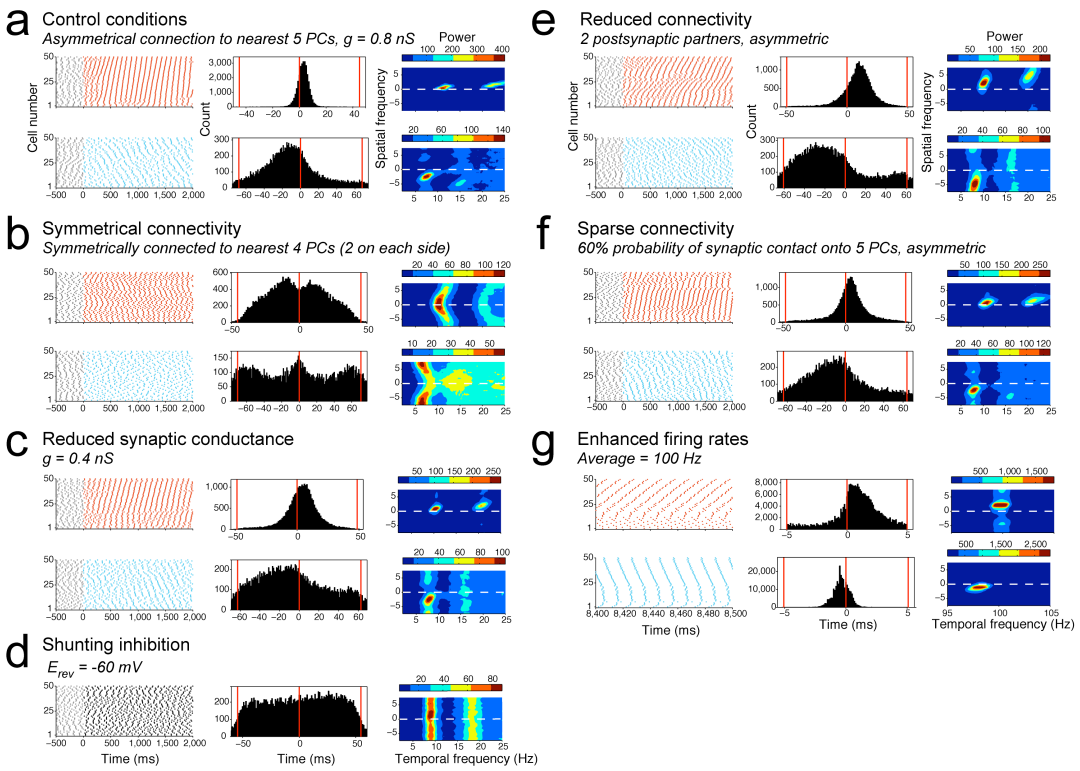

Supplementary Figure 5. Exploring model robustness

The model parameter space was explored to determine the robustness of the traveling waves. Each parameter was titrated; examples of the most divergent parameters examined are shown. In each case, raster plots (left), chain delay analysis plots (middle) and 2D FFT analysis plots (right) are shown for depolarizing synapses (top, E_{rev} = –40 mV) and hyperpolarizing synapses (bottom, E_{rev} = –80mV; see **Supplementary Methods**). In the raster plots, synapses are turned on at time zero. (**a**) Tuned model conditions are shown to facilitate comparison between conditions (**b**) Asymmetric connections are essential for traveling waves, since symmetric connectivity did not produce traveling waves. The broad, symmetrical peaks observed in the chain delay and FFT suggest that waves were standing. (**c**) Traveling waves were robust even when synaptic strength was dramatically reduced. Here, a 2-fold reduction of synaptic conductance still produced traveling waves. (**d**) The synaptic reversal potential did not just determine the wave direction, but also whether or not waves emerged from the network (cf. Ref. 4). When connected by shunting inhibition, the network produced no traveling waves. Note how the 2D FFT (right) resembles that of the unconnected network (Fig. 5d). (**e**) Even when the network connectivity was reduced (asymmetrical connection to 2 nearest neighbors), traveling waves occurred. (**f**) The traveling waves were still robust even when the network was only sparsely interconnected (each Purkinje cell was connected asymmetrically to the nearest 5 Purkinje cells with a probability of 60%). (**g**) Traveling waves were observed when firing rates were enhanced (average firing rate ~100 Hz). Robust waves were seen for both depolarizing and hyperpolarizing synapses, although it took longer for the waves to emerge (raster plot time axis begins 6.4 s after the synapses were turned on).

Nature Neuroscience: doi:10.1038/nn.2285

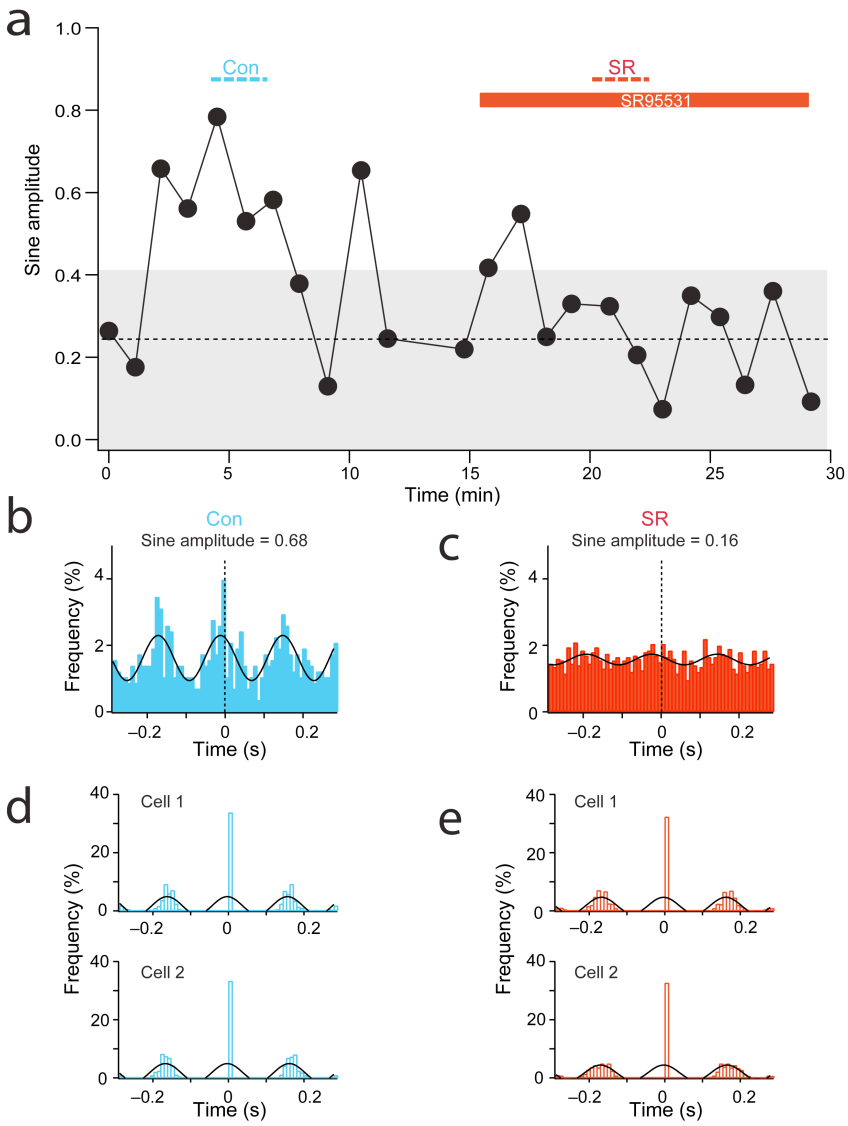

Supplementary Figure 6. Episodic nature of the waves

The waves observed between Purkinje cells in sagittal slices were episodic, as are waves found in other brain regions during development[5]. (**a**) Time course of the cross-correlation between two representative cells showing how cross-correlations waxed and waned. When SR95531 was washed in (red bar), the sine amplitude of the running cross-correlogram was reduced. Average response in SR is shown with dashed horizontal line. Threshold for significant cross-correlation (at $P < 0.05$ level) was determined by bootstrap analysis of SR data, and is illustrated with continuous line. (**b**) and (**c**) show sample cross-correlograms at the times indicated by the colored horizontal dashed lines in panel (a), illustrating a traveling wave (b), and its absence after SR was (c). (**d**) and (**e**) Although the correlated firing between cells was eliminated in SR95531, this was not due to changes in the firing properties of individual cells. Auto-correlograms of two Purkinje cells (top, closer to apex; bottom, more basal) are unchanged after SR is washed in, suggesting that the reduction in the correlation after SR wash-in is not a secondary to changes in the basic firing properties of the cells.

Nature Neuroscience: doi:10.1038/nn.2285

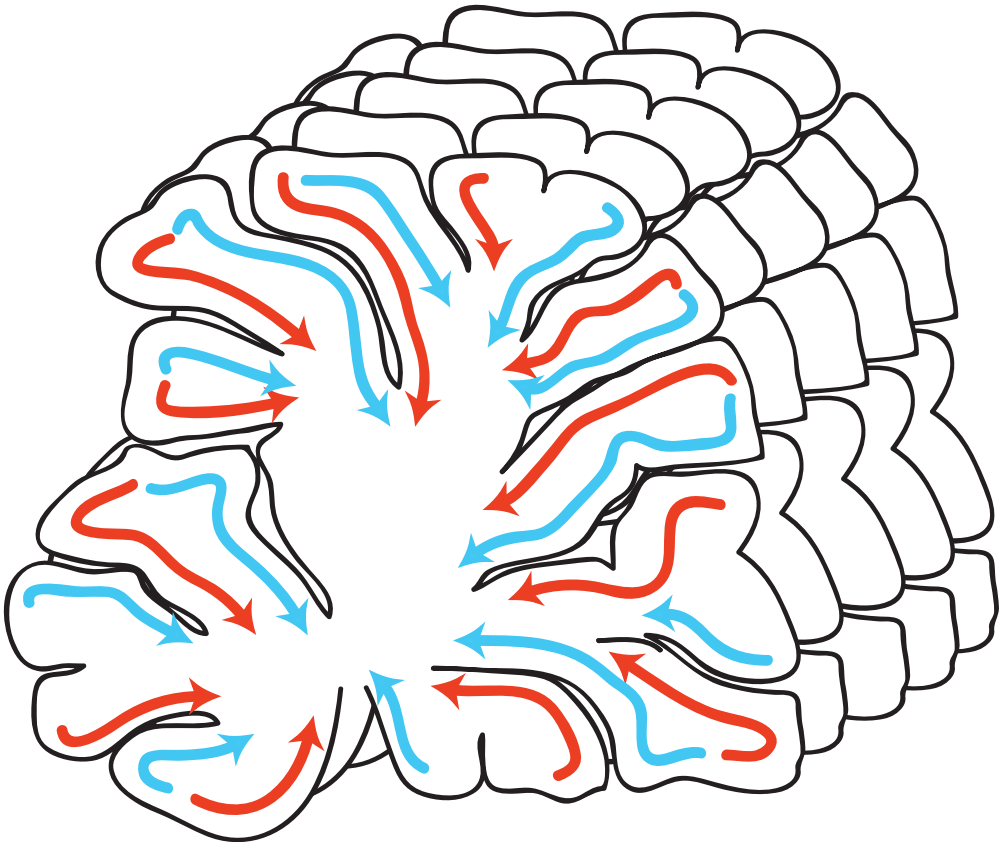

Supplementary Figure 7. Traveling waves define a novel functional unit in the developing cerebellar cortex

A schematic illustration of the functional organization of the juvenile cerebellar cortex described in this study. Purkinje cells form functional units in the sagittal plane defined by their asymmetric collaterals. Thus, in the sagittal plane, each lobule contains two functional units with mirrored symmetry (illustrated here with alternating red and blue arrows). Within each unit, the direction of waves in the lobule depends on developmental stage and on E_{GABA}.

Nature Neuroscience: doi:10.1038/nn.2285

Supplementary Table 1. Synaptic properties of Purkinje-Purkinje connections

	Mean ± s.e.m. (range)
Peak amplitude of PSP	1.9 ± 0.63 mV (0.3 – 8.4)
20–80% rise time of PSP	2.2 ± 0.24 ms (0.7 – 3.9)
Decay τ of PSP	20 ± 1.9 ms (11 – 37)
Latency	0.6 ± 0.05 ms (0.2 – 0.9)
Coefficient of variation	0.9 ± 0.13 (0.4 – 2.9)
Failure rate	33 ± 5% (0 – 78)
Number of putative synaptic contacts	3.7 ± 0.84 (2 – 8)
20–80% rise time of PSC	0.8 ± 0.13 ms (0.5 – 1.6)
Decay τ of PSC	5.8 ± 0.99 ms (1.6 – 10.6)

Peak amplitude, rise time, decay τ and latency values were determined from average PSPs (*n* = 20 pairs). Average PSCs were used to determine rise time and decay τ in voltage-clamp recordings (*n* = 11 pairs). The coefficient of variation and failure rate were determined from an average of 49 ± 5 individual responses. Peak amplitudes include failures; only pairs with symmetrical chloride internal solution were included for peak amplitude measurement (*n* = 14). To permit accurate measurement of decay τ, we used an amplitude cut-off of 0.4 mV (*n* = 17). The number of putative synaptic contacts was determined visually using a 100X high–numerical aperture objective from fixed biocytin-filled neurons in which synaptic connections were confirmed electrophysiologically (*n* = 7; see Supplementary Methods).

Nature Neuroscience: doi:10.1038/nn.2285

Traveling waves in developing cerebellar cortex mediated by asymmetrically connected Purkinje cells

Alanna J. Watt, Hermann Cuntz, Masahiro Mori, Zoltan Nusser, P. Jesper Sjöström & Michael Häusser

Supplementary Methods

Slice preparation, imaging and electrophysiology

All experiments were carried out in accordance with the animal care and handling guidelines approved by the U.K. Home Office. *L7-tau-gfp* mice[6] were used in most experiments. In a few cases, *GAD65-egfp* mice[7, 8] were used. Mice (P3 – P25) were anesthetized with isoflurane, sacrificed, and the brain was rapidly removed into ice-cold artificial cerebrospinal fluid (ACSF, in mM: NaCl, 125, KCl, 2.5; $MgCl_2$, 4; NaH_2PO4, 1.25; $CaCl_2$, 0.5; $NaHCO_3$, 26; dextrose, 25; osmolality 315-320 mOsm, bubbled with 95% O_2/5% CO_2). Acute sagittal slices (200-300 µm) of cerebellar vermis were cut using a VT1000S or VT1200S microtome (Leica Microsystems, Germany) and were transferred to ACSF with the same composition as above, except with 1 mM $MgCl_2$ and 2 mM $CaCl_2$. Slices were incubated for 30 minutes at 37°C and were allowed to cool to room temperature. All experiments were carried out at 33 – 35°C. Patch pipettes (5 – 8 MΩ) for whole-cell recordings were pulled on a DMZ Universal Puller (Zeitz, München, Germany) or a PC-10 puller (Narishige, Japan). Since the Cl^- reversal potential in Purkinje cells is known to shift over the age span that we examined and thus could not be matched easily[9] (see Supplemental Fig. 1), internal solution containing symmetrical Cl^- was used in most recordings. This internal solution also maximized the signal-to-noise of $GABA_A$ receptor-mediated responses. The symmetrical Cl^- internal solution contained (in mM): KCl, 150; K–HEPES, 10; MgATP, 4; NaGTP, 0.3; EGTA, 0.05; and 0.2% w/v biocytin, adjusted with KOH to pH 7.2 – 7.4, and with sucrose to 290 – 295 mOsm. In some cases, EGTA was omitted. For two-photon imaging (see below), 10 – 25 µM Alexa Fluor 594 was added to the internal solution. In a subset of experiments, a low-Cl^- internal solution (E_{Cl} = –82 mV at 34 °C) was used, containing (in mM): K-gluconate, 122; KCl, 3; K-HEPES, 10; $MgCl_2$, 2; MgATP, 2; NaGTP, 0.4; EGTA, 0.05; creatine phosphatase, 10; and 0.02% w/v biocytin, with pH and osmolality as above. In

Nature Neuroscience: doi:10.1038/nn.2285

most voltage clamp experiments, a Cs^+-based internal solution was used, containing (in mM): CsCl, 124; K-HEPES, 10; $MgCl_2$, 4.6; $CaCl_2$, 0.1; NaATP, 4; NaGTP, 0.4; EGTA, 1; and 0.2% w/v biocytin, adjusted with CsOH to pH 7.2-7.4, and with sucrose to 290-295 mOsm. Excitatory synaptic currents were not blocked. In some cases, the $GABA_A$ receptor antagonist SR95531 (gabazine, 10 μM; Sigma-Aldrich or Tocris) was added to the ACSF.

Two-photon imaging was carried out using a custom-built two-photon laser-scanning microscope (Prairie Technologies, Middleton, WI) with a Ti:Sapphire laser (MaiTai, Spectra-Physics) tuned to 890 nm. Putative presynaptic neurons were identified by following the course of intact axon collaterals to potential postsynaptic target neurons. Pre- and postsynaptic neurons were visualized with laser-scanning Dodt-contrast imaging (Dodt tube from Luigs & Neumann, Ratingen, Germany). Data were acquired using ScanImage[10] running in Matlab (MathWorks, Natick, MA, USA), and analyzed with ImageJ (http://rsb.info.nih.gov/ij/). The morphology of Purkinje cells was determined either during the experiment by two-photon imaging of Alexa Fluor 594 fluorescence (at 800 – 840 nm), and/or after the experiments by biocytin histochemistry (Vectastain ABC Elite kit, Vector Labs, Burlingame, CA, USA; see below). Fluorescent images (e.g. Fig. 2a) are pseudocolored maximum intensity projections (rendered using OsiriX, Ref. [11]) of Alexa 594 or GFP fluorescence Z stacks. Whole-cell recordings were obtained using either BVC-700A (Dagan Corporation, Minneapolis, MN) or Multiclamp 700B amplifiers (Molecular Devices, Sunnyvale, CA) controlled by custom made electrophysiology software[12] running in Igor Pro (WaveMetrics Inc., Lake Oswego, OR, USA). Sweeps were filtered at 5 kHz and acquired at 10 kHz using an ITC-18 board (Instrutech, Port Washington, NY, USA). Series resistance and capacitance were compensated (R_{series} < 50 MΩ).

For whole-cell recording, we obtaining giga-ohm seals on up to four neurons that had been previously identified as targets using two-photon imaging, and typically established whole-cell configuration in quick succession to prevent unequal dialysis. Neurons were hyperpolarized to prevent spontaneous firing. APs were evoked by 5-ms-long current injections (1.0 – 2.0 nA) in each neuron every 8 to 15 seconds. All possible connections between recorded cells were tested. Connectivity was assessed by averaging at least 20 traces.

Nature Neuroscience: doi:10.1038/nn.2285

For short-term plasticity experiments, spike trains (3 – 8 pulses) were elicited in the presynaptic neuron at different frequencies (10 – 120 Hz), and these frequencies were interleaved.

Dynamic clamp[13-15] was performed using custom-built analog circuitry. The use of dynamic clamp was necessary because Purkinje – Purkinje synapses are predominantly somatically located (cf. Fig. 2 and Fig. 3) and thus are strongly influenced by somatic action potentials. The synaptic conductance waveform was based on average values obtained with voltage clamp recordings of connected Purkinje – Purkinje pairs (20 – 80% rise time = 0.8 ms; τ_{decay} = 6 ms; see Supplementary Table 1). In individual cells, the peak conductance amplitude was scaled to produce a 2 mV PSP in current clamp for V_{hold} = –70 mV and E_{rev}= 0 mV (cf. Ref. [14]), to match data obtained from monosynaptically connected Purkinje cells in similar conditions (Supplementary Table 1). With this approach, the resulting dynamic clamp peak conductance was 0.88 ± 0.1 nS (n = 8). To provide a control condition, individual Purkinje cells were first allowed to spike freely during a 1 to 4-s-long baseline period, after which the dynamic clamp synapse was turned on (Fig. 4). For each reversal potential setting, 10-50 such sweeps were repeated at an inter-stimulus interval of 16 s. Reversal potentials ranged from –85 mV to 0 mV (Fig. 4) and were corrected for a liquid junction potential of 10 mV. When several reversal potentials were examined in a cell, these were approximately randomized. To avoid frequencies at which Purkinje – Purkinje synapses undergo strong short-term depression (Fig. 1), the simulated presynaptic firing was kept at 5 Hz (although similar results were obtained at 13 Hz; data not shown). Postsynaptic firing rates ranged from 3 to 8.5 Hz (6.0 ± 0.3 Hz, n = 19). To maintain a constant postsynaptic firing rate, steady holding current was sometimes applied. To minimize the impact of background activity, the chloride reversal of the internal solution was set to E_{Cl} = –55 mV for dynamic clamp experiments. Cross-correlograms were normalized to their total area to show percentage spike counts (frequency %) on the ordinate and a sinusoid was fit (Igor Pro). During the baseline period (cf. Fig. 4b, c; inset top right), cross-correlograms were calculated for 5 Hz presynaptic firing with zero synaptic conductance (“synapse off”). The phase in Figure 4e, ϕ, was measured as the x-axis location of the cross-correlogram

Nature Neuroscience: doi:10.1038/nn.2285

center peak (cf Fig. 4b, c; inset bottom right) expressed in terms of radians of the presynaptic firing cycle.

For extracellular recordings, slices were prepared as above from P4 – P6 mice (young) or P17 – P22 mice (old), with excitatory synaptic currents blocked with DNQX (Sigma-Aldrich), although waves were also observed in a subset of recordings made without AMPA receptor blockade (n = 3, data not shown, young animals). Pipettes were the same size as those used for whole-cell recording, but were filled with external solution. Sweeps were acquired at 10 – 20 kHz and filtered at 3 kHz. Depending on the shape of the AP waveform and signal-to-noise of the recordings, AP detection was done either with template matching or with thresholding. Cross-correlograms were measured as above. As the waves are episodic (see Supplementary Fig. 6), the maximal sine wave peak amplitude is reported for each case with at least 400 AP pairings, corresponding to between 2 and 20 sequential traces (12 – 100 s long). A bootstrap approach was used for each pair of recordings to assess the significance of the observed correlation (see statistics below). The phase in Figure 6d, ϕ, was measured as described above for conductance clamp.

GABA puffing and determination of Purkinje cell firing rate

Slices were made from P3 – 37 *L7-tau-gfp* mice as described above. Perforated patch recordings of Purkinje cells were made using gramicidin (Sigma-Aldrich) and GABA was focally applied to the soma while the postsynaptic holding potential was varied to determine the GABA reversal potential. The ACSF was as above and included CNQX (10 μM) and APV (50 μM) to block excitatory synaptic transmission. Recording electrodes (4 – 6 MΩ) were tip-filled for 2 – 5 s with a K^+-based internal solution (see above). They were then back-filled with the same internal solution containing 25 – 50 μg/ml of gramicidin (from a stock solution dissolved in DMSO). Gramicidin-containing internal was made fresh for each attempted recording, and the stock solution was remade regularly. After a GΩ seal was made, perforation was typically achieved within 5 – 25 min. If perforation was not achieved after 30 min, the cell was discarded and fresh gramicidin-internal solution was made.

Nature Neuroscience: doi:10.1038/nn.2285

Perforation was assayed by measuring the R_s throughout the experiment in response to a small hyperpolarizing voltage step. GABA application was started when $R_s \leq 50$ MΩ. GABA (10 μM in ACSF) was applied using a picrospritzer (5 – 15 psi). Data were collected at 20 kHz and filtered at 4 – 10 kHz using a Digidata 1321A board with pClamp software. GABA reversal potential was calculated from the x-axis intercept.

Laser ablation

Optical lesioning was performed using high power levels of pulsed Ti:Sapphire laser light (λ = 890 nm)[16, 17] targeted using our two-photon microscope. A region along the bank of a lobule midway between two extracellular recordings was selected, and a strip perpendicular to the Purkinje cell layer spanning the depth of the granule cell layer was targeted. The average laser power under the objective was increased from ~10 mW during imaging to ~65 mW during ablation. Using frame scan mode (1 ms/line, 7.4 fps), a 30 μm X 30 μm area was manually focused throughout the tissue while being simultaneously monitored using laser-scanning Dodt contrast imaging. Typically, tissue damage (easily visible as an increase in autofluorescence; see Fig. 7b) became visible within seconds on the most superficial part of the slice. However, tissue appeared undamaged at depths of ~100 μm or more, suggesting that collaterals below this depth probably remain intact. In a subset of experiments, Purkinje cell axon collaterals were severed with surgical scissors (n = 2). We obtained indistinguishable results with the two different ablation procedures, so the data were pooled.

Data analysis and statistics

Electrophysiological data were analyzed using custom-written analysis software running on Igor Pro. Curve fits were done by least-square gradient descent in Igor Pro. Data are reported as means ± s.e.m., unless otherwise indicated. Comparisons were made using either paired, two-tailed Student's t–tests or unpaired two-tailed Student's t–tests assuming unequal variances. To correct for multiple comparisons, we used single-factor ANOVAs followed by post-hoc Tukey HSD tests, which were confirmed with the Bonferroni–Dunn method. For multiple comparisons, P values reflect the result of the Tukey

Nature Neuroscience: doi:10.1038/nn.2285

HSD test; ANOVA values were significant to < 0.0001. To compare the rates of traveling wave occurrence, the Wilcoxon rank sum test was used on sinusoid amplitude ensemble data sets.

The statistical significance of cross-correlations was assessed using a bootstrap approach[18]. This method was essential to accurately distinguish between real and spurious correlations in the case of the older animals, which are more prevalent due to elevated firing rates in older Purkinje cells[19, 20]. To numerically populate the analytically unknown distribution of cross-correlation amplitudes, experimentally recorded spike trains were divided into 6 to 20 segments that were randomly shuffled and flipped in time. For each draw of two spike trains, a cross-correlation was calculated, a sinusoid was fit (cf. Fig. 4, 6, 7), and its amplitude was recorded. Draws were repeated 500 times. Based on this numerically generated distribution, the statistical significance of the cross-correlation amplitude was assessed at the $P < 0.05$ level. The distribution was repopulated for each paired extracellular recording, thus inherently controlling for differences in firing rate and CV across recordings. The bootstrap approach was tested on connected and unconnected versions of the tuned network model and predicted connectivity with high accuracy.

Confocal and electron microscopy

Six *L7-tau-gfp* mouse pups (P8 or P18) were transcardially perfused first with 0.9% saline for 1 minute followed by a fixative containing 2% paraformaldehyde (PA) and 0.5% glutaraldehyde (GA) in 0.1M Na-acetate buffer (pH = 6) for 2 minutes, then 2% PA and 0.5% GA in 0.1 M Na-borate buffer (pH = 8) for 1 hour. The following day, 60 µm sagittal sections were cut from the vermis with a Vibratome and were collected in 0.1 M phosphate buffer (PB). Following treatment with 1% Na-borohydrate for 10 minutes, the sections were blocked in Tris-buffered saline (TBS) containing 10% normal goat serum (NGS) for 30 minutes. The sections were incubated in the solution of primary antibodies (mouse monoclonal anti-GFP, Abcam, Cambridge, MA, Cat. No. ab1218; and rabbit anti-GFP, Chemicon, Temecula, CA, Cat. No. AB3080P; made up in TBS containing 2% NGS and 0.05% TritonX100; both diluted at 1:500) overnight. For double immunofluorescent reactions, sections were incubated in rabbit anti-GFP (1:500) and guinea pig anti-vesicular

Nature Neuroscience: doi:10.1038/nn.2285

inhibitory amino acid transporter antibodies (Calbiochem, EMD Chemicals, San Diego, CA; Cat. No. 676780, 1:500). After several washes, the sections were either treated with Alexa Fluor 488-coupled goat anti-mouse or anti-rabbit IgGs (Molecular Probes, Eugene, OR), Cy3-coupled goat anti-guinea pig IgG (1:500 Jackson ImmunoResearch Laboratories, West Grove, PA) or in 0.8 nm gold-coupled goat anti-mouse or anti-rabbit IgGs (Aurion, Wageningen, The Netherlands). Sections of the fluorescent reactions were coverslipped and mounted in Vectashield (Vector Lab, Burlingame, CA, USA). Immunogold EM was used to allow us to unequivocally identify presynaptic Purkinje cell axon terminals at the ultrastructural level, since previous EM studies using a variety of presynaptic markers have produced conflicting results about the existence of Purkinje – Purkinje cell synapses[21-26]. Ultra-small gold particles were silver enhanced (EM-SE kit) as described by the manufacturer (Aurion). Sections with immunogold reactions were dehydrated, stained with uranyl acetate followed by lead citrate and were embedded in Epoxy resin. Fluorescent reactions were analysed with a confocal laser-scanning microscope (Olympus FV1000). Images were acquired with a 60x high NA (1.35) objective. Sixty-nm-thick electron microscopic sections were prepared and analyzed with a Jeol TEM1011 microscope.

Neurolucida reconstructions

In functionally connected pairs of neurons, putative synaptic contacts were visualized using bright-field microscopy with a 100x oil immersion objective (1.3 NA, Olympus BX51, Olympus, Melville, NY) of neurons histologically processed for biocytin. Synaptic contacts were defined as presynaptic axonal swellings in close proximity (<1 µm separation) to the postsynaptic cell. To improve visualization of the biocytin-labelled axon in three dimensions as it wrapped around the postsynaptic Purkinje cell soma, we chose pairs where postsynaptic Purkinje cells were relatively lightly stained, which aided identification of putative synaptic contacts. Purkinje cells and their axons were digitally reconstructed using Neurolucida (MicroBrightField Inc., Magdeburg, Germany).

The projection pattern of Purkinje cell collaterals was quantified using custom software running in Matlab. Reconstructed Purkinje cells were first cantered

Nature Neuroscience: doi:10.1038/nn.2285

on their somata and their main axons were aligned in three dimensions such that the white matter was down and the direction away from the lobule apex was to the right. A two-dimensional axon collateral density projection onto the sagittal plane was then generated. The apex-base direction was confirmed by examining the position of the Purkinje cell within the slice.

Network model

The simulation of the Purkinje cell network was implemented in NEURON[3]. 50 point neurons, corresponding to 1 mm of folium divided by 20 μm distance between the centers of neighboring Purkinje cell somata, incorporating voltage-dependent conductances found in cerebellar Purkinje cells[2], were arranged in a one-dimensional lattice. The membrane surface area of the original model, which was based on dissociated Purkinje cell properties[2], was increased by a factor of 13 in order to obtain an input resistance similar to that of Purkinje cells in cerebellar slices (about 80 MΩ), without affecting the spiking behavior since it is a point neuron model. The cells were connected to the subsequent five cells in the chain. The synaptic properties were allocated in accordance with the experimental results. The peak synaptic conductance was 0.8 ± 0.2 nS (mean ± s.d.) with reversal potentials of either –80 ± 2.5 mV ("hyperpolarizing") or –40 ± 2.5 mV ("depolarizing"), and followed a bi-exponential time course with τ_1 = 0.5 ± 0.2 nS and τ_2 = 2.5 ± 0.5 ms. For each cell, the values describing the synaptic conductance were drawn from normal distributions with mean and standard deviation as indicated. Since collateral path length did not correlate with distance between Purkinje cell somata (data not shown), synaptic delay times (0.6 ± 0.05 ms) were not tuned differently for connected pairs separated by small or large distances. The network simulations were performed at the firing rates typical for the age of the animals used in this study; the basic results are similar over a wide range of firing rates (Supplementary Fig. 5). The impact of a repetitive synaptic stimulation on entraining a postsynaptic cell firing was calibrated on the data obtained in the dynamic clamp experiments shown in Figure 4 (Supplementary Fig. 3). In order to reproduce the experimental data accurately, a noise source corresponding to intrinsic noise was introduced in the model: at each time step of the simulation a current injection amplitude

Nature Neuroscience: doi:10.1038/nn.2285

was drawn from a normal distribution around 0 pA mean with a standard deviation of 2 pA reproducing the CV of interspike intervals of around 0.1 (as measured in Ref. [27]). The corresponding distributions of firing rates in the connected network were set to approximately match the experimentally observed values (see Supplementary Fig. 1), using hyperpolarizing bias current (–35 ± 0.05 pA), giving firing rates of 11.3 ± 1.1 Hz for the case of depolarizing synapses and 7.3 ± 1.4 Hz for the hyperpolarizing case (mean ± s.d.). The phases of all cells were perturbed randomly and separately at the beginning of each trial. The simulations ran for 10 sec with a time step of 0.025 ms. The connection was turned on after 1500 ms. Waves appeared after a few 100 ms depending on the network parameters (see Supplementary Fig. 5). Each presented parameter set was run 11 times, and the parameters from the network model were drawn anew each trial, according to the distributions described above. The data obtained from the simulations in NEURON were processed in Matlab. Movies of the raster plots were obtained by playing the spike trains after heavy temporal filtering into the schematic illustration of the Purkinje cell network visualized using ray-tracing software (http://www.povray.org/). For acoustic monitoring, spikes were fed into a synthesizer according to their timing and to the cell number in which they occurred: low pitch = closer to lobule apex; high pitch = more basally in the lobule. The angular spectrum decomposition (used in Fig. 5d – f and Supplementary Fig. 5) was obtained by performing a simple 2D FFT directly on the binary raster plots. Contour plots were drawn with 5 levels.

We examined the robustness of the waves in the model using two independent methods (Supplementary Fig. 5). The existence of waves was robust to drastic changes in the network model: decreasing the connection strength by 50%, connecting only to 2 next neighbors, connecting to the next 5 neighbors with a probability of only 60% in each case, and increasing the variance to mean ratio in the steady state drive dramatically, did not prevent the emergence of propagating waves (Supplementary Fig. 5). The fundamental principle of wave propagation in the network was further validated in a simpler model with 40 integrate-and-fire neurons connected in a similar way in Matlab (data not shown).

Nature Neuroscience: doi:10.1038/nn.2285

To provide further validation of the existence of waves, an additional analysis method was developed: the chain delay. This measures, for each spike, the closest spike in the neighboring cell down the chain, and the time differences between these pairs of spikes are counted in a histogram (Supplementary Fig. 3). In the unconnected network, this histogram of chain delays was flat throughout the time of the inter-spike-interval. In the connected cases the histograms showed sharp peaks on either side of the 0 ms line (Supplementary Fig. 3).

Nature Neuroscience: doi:10.1038/nn.2285

References

1. Paxinos, G. & Franklin, K.B.J. *The Mouse Brain in Stereotaxic Coordinates* (Elsevier Academic Press, 2004).
2. Khaliq, Z.M., Gouwens, N.W. & Raman, I.M. The contribution of resurgent sodium current to high-frequency firing in Purkinje neurons: an experimental and modeling study. *J Neurosci* 23, 4899-4912 (2003).
3. Hines, M.L. & Carnevale, N.T. The NEURON simulation environment. *Neural computation* 9, 1179-1209 (1997).
4. Vida, I., Bartos, M. & Jonas, P. Shunting inhibition improves robustness of gamma oscillations in hippocampal interneuron networks by homogenizing firing rates. *Neuron* 49, 107-117 (2006).
5. Firth, S.I., Wang, C.T. & Feller, M.B. Retinal waves: mechanisms and function in visual system development. *Cell Calcium* 37, 425-432 (2005).
6. Sekirnjak, C., Vissel, B., Bollinger, J., Faulstich, M. & du Lac, S. Purkinje cell synapses target physiologically unique brainstem neurons. *J Neurosci* 23, 6392-6398 (2003).
7. Bali, B., Erdelyi, F., Szabo, G. & Kovacs, K.J. Visualization of stress-responsive inhibitory circuits in the GAD65-eGFP transgenic mice. *Neurosci Lett* 380, 60-65 (2005).
8. Erdelyi, F.*, et al.* GAD65-GFP Transgenic Mice Expressing GFP in the GABAergic Nervous System. in *FENS Meeting* A011.013 (Paris, 2003).
9. Eilers, J., Plant, T.D., Marandi, N. & Konnerth, A. GABA-mediated Ca2+ signalling in developing rat cerebellar Purkinje neurones. *J Physiol* 536, 429-437 (2001).
10. Pologruto, T.A., Sabatini, B.L. & Svoboda, K. ScanImage: Flexible software for operating laser scanning microscopes. *Biomed Eng Online* 2, 13 (2003).
11. Rosset, A., Spadola, L. & Ratib, O. OsiriX: an open-source software for navigating in multidimensional DICOM images. *J Digit Imaging* 17, 205-216 (2004).
12. Sjöström, P.J., Turrigiano, G.G. & Nelson, S.B. Rate, timing, and cooperativity jointly determine cortical synaptic plasticity. *Neuron* 32, 1149-1164 (2001).
13. Sharp, A.A., O'Neil, M.B., Abbott, L.F. & Marder, E. Dynamic clamp: computer-generated conductances in real neurons. *J Neurophysiol* 69, 992-995 (1993).
14. Mittmann, W. & Häusser, M. Linking synaptic plasticity and spike output at excitatory and inhibitory synapses onto cerebellar Purkinje cells. *J Neurosci* 27, 5559-5570 (2007).
15. Robinson, H.P. & Kawai, N. Injection of digitally synthesized synaptic conductance transients to measure the integrative properties of neurons. *J Neurosci Methods* 49, 157-165 (1993).
16. Yanik, M.F.*, et al.* Neurosurgery: functional regeneration after laser axotomy. *Nature* 432, 822 (2004).

Nature Neuroscience: doi:10.1038/nn.2285

17. Mejia-Gervacio, S.*, et al.* Axonal speeding: shaping synaptic potentials in small neurons by the axonal membrane compartment. *Neuron* 53, 843-855 (2007).

18. Efron, B. Nonparametric estimates of standard error: The jackknife, the bootstrap and other methods *Biometrika* 68, 589-599 (1981).

19. Brody, C.D. Correlations without synchrony. *Neural computation* 11, 1537-1551 (1999).

20. de la Rocha, J., Doiron, B., Shea-Brown, E., Josic, K. & Reyes, A. Correlation between neural spike trains increases with firing rate. *Nature* 448, 802-806 (2007).

21. Chan-Palay, V. The recurrent collaterals of Purkinje cell axons: a correlated study of the rat's cerebellar cortex with electron microscopy and the Golgi method. *Z Anat Entwicklungsgesch* 134, 200-234 (1971).

22. Larramendi, L.M. & Lemkey-Johnston, N. The distribution of recurrent Purkinje collateral synapses in the mouse cerebellar cortex: an electron microscopic study. *J Comp Neurol* 138, 451-459 (1970).

23. Hamori, J. & Szentagothai, J. Identification of synapses formed in the cerebellar cortex by Purkinje axon collaterals: an electron microscope study. *Exp Brain Res* 5, 118-128 (1968).

24. De Camilli, P., Miller, P.E., Levitt, P., Walter, U. & Greengard, P. Anatomy of cerebellar Purkinje cells in the rat determined by a specific immunohistochemical marker. *Neuroscience* 11, 761-817 (1984).

25. Meek, J. & Nieuwenhuys, R. Palisade pattern of mormyrid Purkinje cells: a correlated light and electron microscopic study. *J Comp Neurol* 306, 156-192 (1991).

26. Pouwels, E. On the development of the cerebellum of the trout, Salmo gairdneri. IV. Development of the pattern of connectivity. *Anat Embryol (Berl)* 153, 55-65 (1978).

27. Häusser, M. & Clark, B.A. Tonic synaptic inhibition modulates neuronal output pattern and spatiotemporal synaptic integration. *Neuron* 19, 665-678 (1997).

Nature Neuroscience: doi:10.1038/nn.2285